



Experimental study of flapping-wing aerodynamic coefficients and landing performance estimation

Saeed Karimian Aliabadi ·
Mohamad Reza Parsa · Majid M. Moghadam

Received: 10 April 2022 / Accepted: 7 February 2023 / Published online: 5 March 2023
© Springer Nature B.V. 2023

Abstract In this research, a typical flapping-wing air vehicle is fabricated and tested in a wind tunnel to explore the effect of kinematic parameters on the aerodynamic forces and moments. Moderate and high incidence angles are considered to estimate the hover and landing performance of the birds. Flapping kinematics consisting of frequency and amplitude, velocity, incidence angle, and body pitch rate are assumed as the state. The aerodynamic forces and moments are also measured in each state via a force balance. A comprehensive experimental parameter study of a flapping-wing micro air vehicle (FMAV) is depicted, and some new remarks are drawn. Increasing the angle of attack would make a higher lift while diminishing the axial force required in the perching maneuver. The force hysteresis study reveals that increasing flapping frequency and angular velocity may lead to dynamic instability due to lag and deficiency effects. A semi-analytical aerodynamic model is developed to further estimate the landing scenario based on the conducted experiments. Based on the smooth descending transition, a quasi-equilibrium trajectory is proposed by which the flapping robot could approach the landing configuration from the initial cruise condition. It is shown that by controlling both frequency and pitch angle, the bird's velocity and

altitude would reach from 9 m/s and 12 m to 3 m/s and 1 m, respectively, which is suitable for the terminal landing maneuver.

Keywords Flapping-wing vehicle · Aerodynamic forces and moments · Wind tunnel test · Dynamic balance · Flapping kinematics · Descend trajectory

1 Introduction

Bird and insect flight has captured the attention of many researchers in the last two decades. Based on the evidence in nature, it has been found that flying is one of the most successful methods of movement among living things. With this in mind, scientists and engineers have studied birds to discover new ideas for designing human-crewed and unmanned aircraft. Such studies have been conducted on issues such as bird hovering, navigation, and group flight [1]. One of the recent efforts of engineers and scientists has been to make artificial ornithopters inspired by birds. Ornithopters produce lift and thrust power to fly like wing flapping in birds. The Nano Hummingbird is one of the most successful artificial birds. It has a mass of 19 g, a wingspan of 16.5 cm, and hovering capability for several minutes to fly forward at 6.7 m/s and transmit a live color video to a remote ground station [2].

The Delfly [3, 4] is a flapping-wing micro air vehicle (FMAV) built at Delft University of Technology. Delfly FMAVs are well-studied platforms. Several

S. K. Aliabadi (✉) · M. R. Parsa · M. M. Moghadam
Mechanical Faculty, Tarbiat Modares University, Tehran,
Iran
e-mail: Karimian@modares.ac.ir

versions, such as Explorer and Nimble, are the collections of these flapping wings. The wingspan of these FMAVs is between 10 and 50 cm, and their weight is between 3.07 and 21 g. Other flapping wings that have flown successfully are RoboRaven and Arizona University flapping wings [5, 6]. All of the above flapping wings have differences in structure, and none of them is optimal compared to real birds. Researchers have made great efforts to find an appropriate structure. For example, Mueller et al. [7] developed a passive, spatially distributed, one-way folding mechanism. This mechanism has been incorporated into a flying MAV test bed, and the MAV has successfully shown flying ability at reduced forward velocity while maintaining the payload carrying capacity.

Stewart et al. [8] achieved a multi-objective optimization method on the shape of a rigid flapping wing to reduce the peak of input power and increase the cyclic mean thrust. Guerrero et al. [9] presented a preliminary design of a biologically inspired flapping unmanned aerial vehicle (FUAV). The proposed model was used to assess the aerodynamic performance and longitudinal static stability of the FUAV in gliding and flapping conditions. The study's results give us an initial insight into the aerodynamic performance and longitudinal static stability of a biomimetic flapping UAV, designed at minimum flight velocity and maximum flapping frequency. Negrello et al. [10] addressed the design of the actuating mechanism of a biologically inspired flapping wing UAV. They conducted an optimization study to select the best configuration to reproduce the desired flapping-wing kinematics. Furthermore, a structural and durability analysis was conducted to verify that the mechanism and its components could withstand the aerodynamic and inertial loads.

Nian et al. [11] designed a flapping wing with an attached airfoil to the root. EPPLER 378 and EJ 85 airfoils were used to test the flapping wing. The tests showed that the cruise velocity envelope was expanded, especially with a small cruise velocity. However, the airfoil attached to the root could cause a slight decrease in the endurance and range of the flapping wing. The wing structure of conventional flapping wings (membrane flapping wings) consists of a carbon fiber skeleton with bird-like curves covered by a light Mylar/cloth skin. This structure ensures proper deformation during flapping to produce the required forces. It also reduces the inertial forces of periodic

accelerations due to minimum weight. Since the center of mass, aerodynamic center, and shear center do not coincide in these membrane wings, forces and moments produced by flapping would result in both twisting and bending. It would also cause the angle of attack (AOA) and relative velocity distribution to be highly varied along the wingspan.

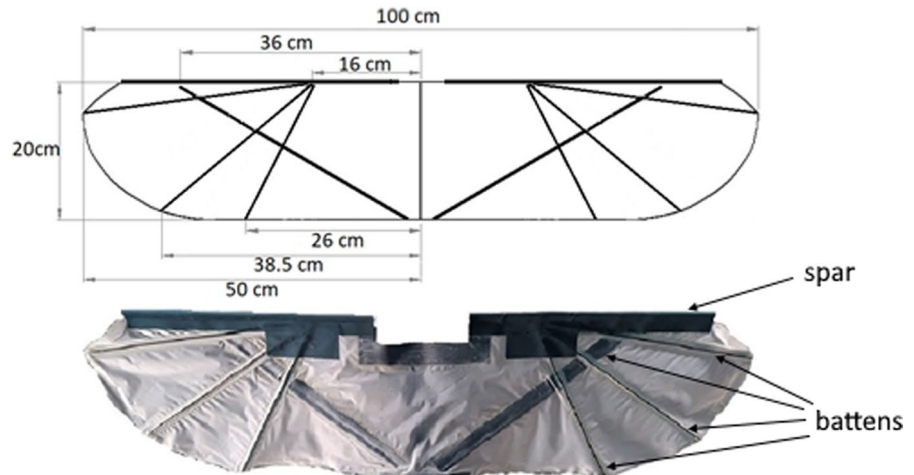
There are several underlying physics phenomena in the aerodynamics of flapping wings: leading-edge vortex, wake capture, near fling,¹ and apparent mass [6]. Many activities, including experimental [12–14] and numerical [15, 16] studies, have explored the complex aerodynamic phenomena occurring during flapping flight. Measuring the forces and moments of flapping wings in wind tunnels and visualizing the flow in wakes behind flapping wings have been reported.

Many experimental studies have been performed to optimize or modify the average forces and moments. Gallivan and DeLaurier [17] conducted an experimental study to reveal the effect of the wing aspect ratio, wing shape, spar stiffness, wing mass, and skeleton arrangement. Lift, thrust, and pitching moment characteristics were measured and then averaged in a flapping cycle for only two angles of attack at 0 and 10 deg. In another experimental study, Shkarayev and Silin [6] examined other parameters such as wing size and reduced frequency for a broader AOA range (0–90 deg).

Perching can be defined as landing on a specific point with approximately zero horizontal and vertical velocity. To perform this type of landing, birds use several specific maneuvers. They begin to flap their wings at a high frequency in a short period to produce additional lift as the forward velocity decreases. At the same time, they rotate their body and wings to high AOA (even close to 90 deg). This rotation increases the drag, thereby further decreasing the velocity. The question is how the presence of the

¹ One of the particular mechanisms to generate lift in birds is the "clap and fling." The clap and fling mechanism consists of two phases: (1) the leading edges of both wings clap together at the end of the upstroke, and (2) the wings rotate around their trailing edges and fling apart. During the "fling" phase or the down stroke, air flows around the leading edge of each wing, which creates a bound vortex on each wing, acting as the starting vortex for the opposite wing. This allows a rapid buildup of circulation and an increase in total lift production.

Fig. 1 Geometry of wing



AOA rate ($\dot{\alpha}$) may affect the forces and moments. Karimian and Jahanbin have presented a Bond Graph model for a typical FMAV and performed a lateral parameter study with the emphasis on control power [18, 19].

To date, perching maneuvers in flapping robots have not been significantly studied. The studies on this maneuver mainly involved fixed wings. Wickenheiser and Garcia [20, 21] investigated the perching maneuver for a morphed vehicle. They designed the optimal trajectory for this maneuver using only the longitudinal dynamics. Hoburg and Tedrake [22], Cory and Tedrake [23], and Moore and Tedrake [24] investigated the capability of using a linear model to control a fixed-wing perching at a specified point. The stability was not addressed in these works.

In [25] and [26], the aerodynamic model of perching was studied in a fixed-wing drone. The vehicle was considered a rigid body, and the lateral or directional dynamic was diminished. The aerodynamic modeling was derived by system identification. The aerodynamic model covered a wide AOA range, including pre-stall and post-stall. Rich and Albertani [27] introduced a first-order time delay aerodynamic model for perching maneuvers using wind tunnel measurements. The model was a fixed-wing that could be twisted in the root and the middle part of the wing. Two series of static and dynamic tests were demonstrated.

Static aerodynamic derivatives have been estimated in almost all experimental studies. The results of these studies could be only used in cruise or hover flight phases. Other flight phases such as

take-off, landing, and turning, have not been adequately addressed in flapping robots. This critical gap was addressed in the present study. The experimental study of the aerodynamic forces and moments during the perching maneuver was the main purpose achieved in the current work. Two categories of static and dynamic tests were defined in the wind tunnel. The parameters studied in the static test were AOA, flapping frequency, flapping amplitude, and wind velocity. The effects of all the mentioned parameters were measured on the aerodynamic coefficients. In the dynamic test, the pitch rate was also investigated. The difference between the dynamic and static results was argued, and a sample typical smooth descent trajectory was extracted based on the quasi-steady analysis.

2 Fabricated wing and flapping mechanism

Aerodynamic force measurements were conducted for a flapping wing with a wingspan of 100 cm. The flapping wing mechanism consisted of a DC motor, a motor speed controller, a mounting rib, a

Table 1 Specifications of flapping wing

Wingspan b , cm	100
Flapping frequency f , Hz	0–7.5
Flapping angle amplitude ϕ , deg	54
Wing area S , m ²	0.28
Mass, g	176



Fig. 2 Constructed FMAV and its main parts

Fig. 3 Wind tunnel setup



gearbox, a tail, and wings. The wing geometry is shown in Fig. 1. Other technical information regarding the flapping wing is given in Table 1. The wing structure consisted of the front spar, battens, and the membrane. The spar was a carbon tube with an outer diameter of 5 mm and an inner diameter of 3 mm. The battens were made of carbon rods with a diameter of 2 mm. The battens were not rigidly fixed to the front spar, which caused pitching deformations of the membrane due to the effect of the inertial and aerodynamic forces.

A typical flexible FMAV,² as shown in Fig. 2, is primarily composed of a fixed body, flapping wings, a servo-controlled tail, and a flapping mechanism gearbox with an electric motor and battery. As a natural consequence of the flapping motion of the elastic wing, a net forward force will be produced, even at zero incidence angle. The wing structure is composed of two main spars: One is installed at the leading edge and the other is crossed. Also, several chord-wise or inclined ribs made of carbon fiber would keep the

planar form. The wing surface is covered by a Mylar skin.

3 Experimental setup

3.1 Wind tunnel facility

Experimental studies were performed in the aeronautical research center wind tunnel (Fig. 3). It is a subsonic, open loop wind tunnel with a 1.8×2 m test section. It can operate in the velocity range from 3 to 20 m/s. Wind flow was laminarized to less than

0.4% turbulence in the settling chamber in the axial direction. Unsteady/transient lift, thrust forces, and pitching moment characteristics were measured using a Mini40 ATI force/torque sensor. The data acquisition system is capable of sampling at 10 kHz. This force balance can measure normal force up to 240 N, horizontal force up to 80 N, and moment up to 4 N.m. Two different measurement stands were used to handle the static and dynamic tests.

3.2 Static and dynamic balance

In a static stand, the force resolution is 0.02 N horizontally and 0.04 N vertically. The moment resolution is 0.0005 N m. The zero drift when an oscillatory load was applied through the flapping wings operating at 6 Hz did not exceed 2.5% per 8 min of the test run. The hysteresis, non-repeatability, and non-linearity of this sensor are below 0.1%. The resonant frequency of this sensor is 4900 Hz in the moment axis and normal force axis and 3200 Hz in the horizontal axis, well above the flapping frequencies. The signal-to-noise ratio in force balance is 75 times

² Flapping wing micro air vehicle.

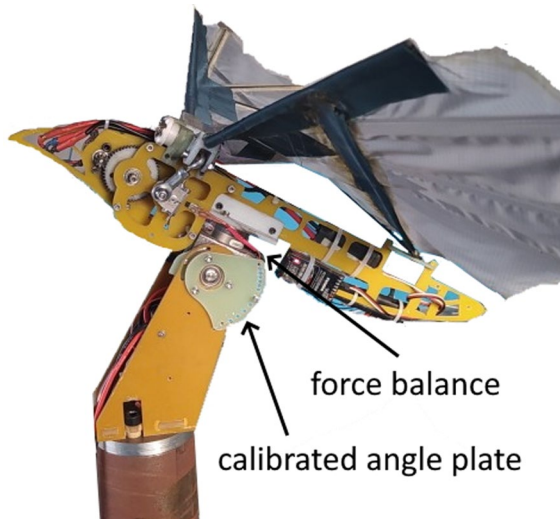


Fig. 4 Static test stand

stronger when using silicon strain gages rather than conventional foil gages. This signal, after amplifying, would result in near-zero noise distortion. Flapping frequency was measured using the ss490 hall-effect sensor.

In the static balance, the aerodynamic forces and moments were measured in the AOA range of 0–90 deg with 3 deg steps using a calibrated angle plate and a pin, according to Fig. 4. In these experiments, it was necessary to calibrate the force balance to cancel the gravity force in zero wind velocity before each test.

The dynamic test rig consisted of a servo motor, a timing belt, and a pulley to transmit power to the bird's axis of rotation. In this stand, the force balance was the interface between the bird and the rotating plate. The planetary Gearhead Maxon 148,867 with a 500 pulse/turn encoder was selected as the servo motor, capable of producing a maximum torque of 15 N m and a maximum speed of 84 rpm. A timing belt and a pulley of 5 M type with a width of 15 mm were selected. This stand can apply an angular velocity of 500 deg per second (Fig. 5).

4 Experimental test results and discussion

The tests were performed in two general categories: static and dynamic. In static tests, the effects of flapping frequency, AOA, wind velocity, wing

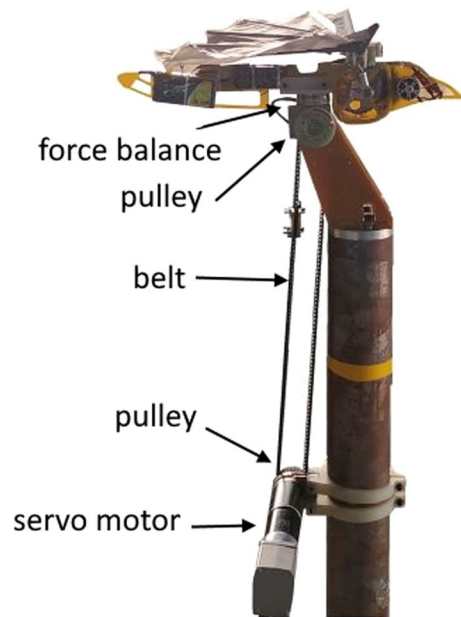


Fig. 5 Dynamic test stand

spar flexibility, and flapping amplitude were investigated on the aerodynamic coefficients. These data are assumed to be a benchmark in dynamic tests. In dynamic tests, the force coefficient results were obtained during the pitching maneuver. The dynamic test variables included flapping frequency, wind speed, and AOA rate ($\dot{\alpha}$).

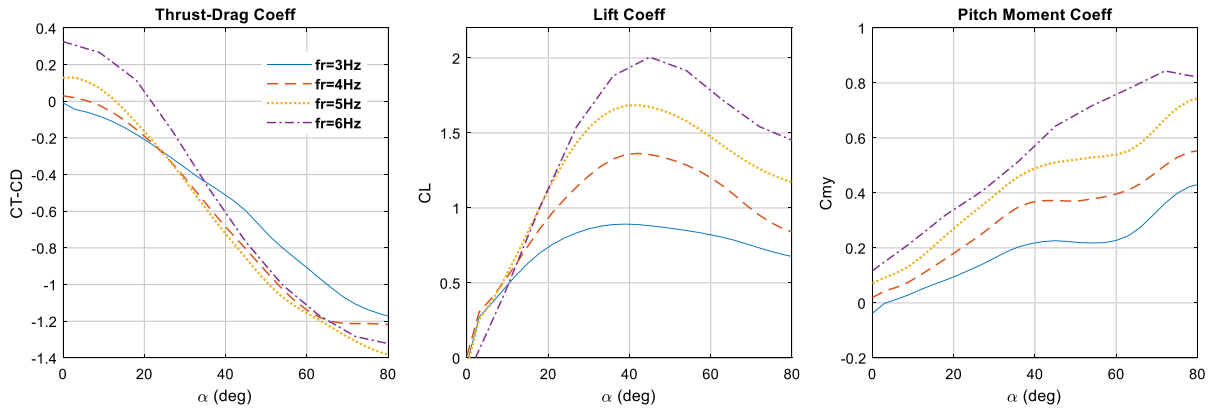
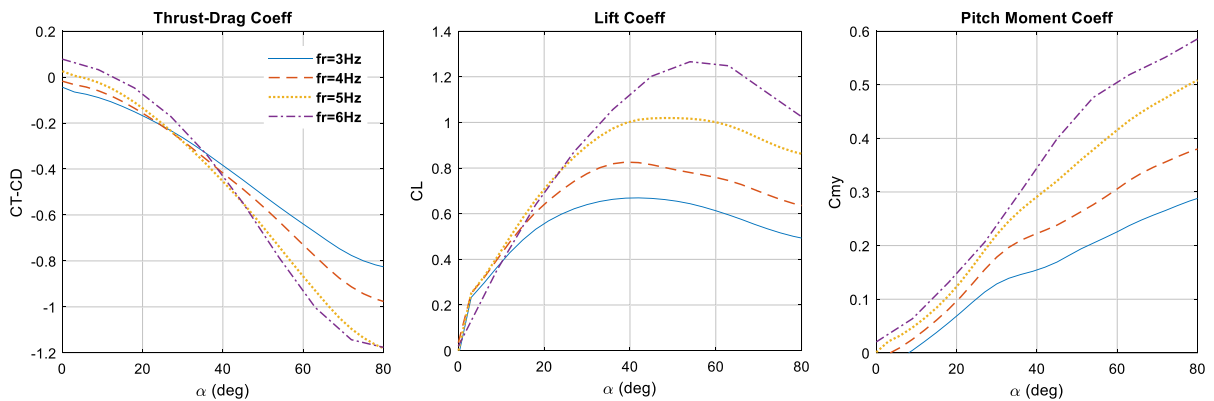
4.1 Static test results

In static tests, axial and normal forces and pitching moment were measured for each body angle from 0 to 80 with 3 deg steps. As mentioned in Table 2, wind speeds of 3, 5, 7.5, and 10 m/s and flapping frequencies of 3, 4, 5, and 6 Hz were examined within two flapping amplitudes of 54 and 72 deg. Two different wing spars were tested (Table 2). According to these variables, more than 2500 tests were performed, and data related to them were recorded. In each test, force and moment data were collected for 7 s.

Since the longitudinal maneuver was considered in this research, two components of axial and vertical forces and pitching moment were captured. In each static test, the average value of the force and moment coefficients was calculated. Due to the force balance being connected to the body and moving with

Table 2 Static test variables and their variation range

Angle of Aattack (α)	Frequency (f)	Velocity (V) (m/s)	Flapping angle amplitudes	Wing spar stiffness
0–80 (deg)	3–4–5–6 (Hz)	3–5–7.5–10 (m/s)	54 (low range), 72 (high range)	Rigid and flexible

**Fig. 6** Forces and pitching moment coefficient on bird regarding angle of attack in Reynolds number of 75,000 and variable frequencies (low flexibility and flapping angle amplitudes of 54 deg)**Fig. 7** Forces and pitching moment coefficient on bird regarding angle of attack in Reynolds number of 112,000 and variable frequencies (low flexibility and flapping angle amplitudes of 54 deg)

it, forces and pitching moment were recorded in the body coordinate system and then converted to the wind coordinate system. Since the landing maneuver usually takes place in a wide angle range, static tests were scheduled in 0–80 AOA intervals.

4.1.1 Effects of the flapping frequency

In Figs. 6 and 7, the aerodynamic coefficients are plotted for a constant velocity of 5 and 7.5 m/s,

respectively, for low amplitudes and high stiffness wing. The first graph in this figure is the difference between thrust drag coefficients. Thrust is created by the flapping mechanism, and the measured axial force is, in fact, the resultant of thrust and drag. It is observed that with increasing flapping frequency, the axial force coefficient increases at low angles of attack. However, this trend is reversed from the attack angle of approximately 30 deg. Increasing the flapping frequency in the inclined attitude

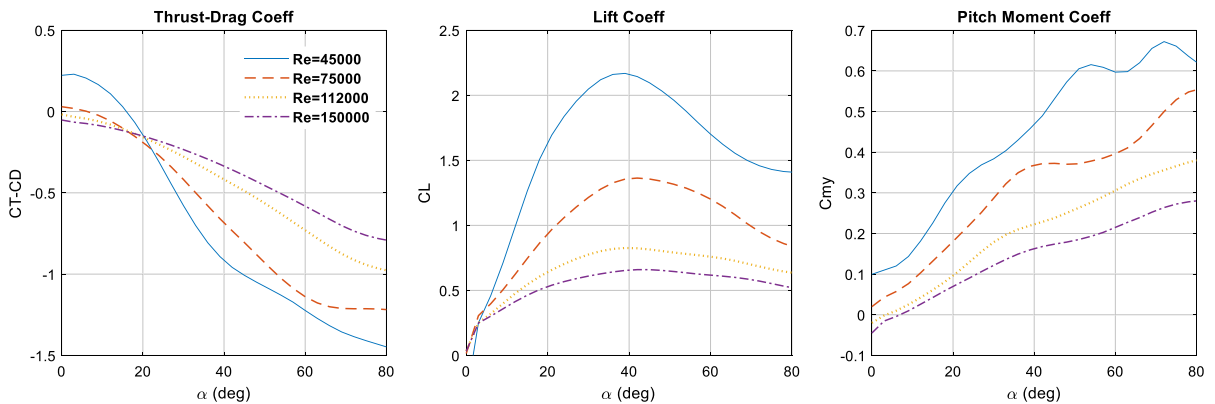


Fig. 8 Forces and pitching moment coefficient on the bird in terms of constant flapping frequency of 4 Hz and variable Reynolds number (low flexibility and flapping angle amplitudes of 54 deg)

raises drag instead of thrust. It is one of the ways birds can perch in nature. The trend becomes more pronounced at higher wind speeds (Fig. 7). With increasing wind speed, the switching AOA would increase.

A similar but reverse trend is observed in the normal force coefficient in angles close to zero; the lift force decreases with increasing flapping frequency, but for the higher angles, the average lift coefficient follows the frequency. The switching angle is approximately 10 deg in the wind speed of 5 m/s. One reason is the change in the direction of the output flow jets during the flapping. As AOA increases, flow jets rotate from the axial to the normal direction.

Because a sudden drop in the lift coefficient graph is not visible, the stall AOA is not found in the graph for the flapping bird. The reason can be the increase of dynamic pressure when the wing rises in flapping motion and prevents the complete separation of the flow from the wing. The trend of this graph is such that it first increases almost linearly and then gradually turns into a curve and reaches its peak point. Next, it decreases with a slope less than the increase of the lift coefficient for initial AOA. As the flapping frequency increases, the point in which the line converts to a curve and the maximum point occur at higher AOA. Regarding the lift coefficient force, it was also observed that at high AOA, the lift coefficient force increased significantly with increasing flapping frequency.

Regarding the pitching moment coefficient applied to the bird, it can be seen that increasing the wing

flapping frequency and AOA close to 70 deg first increases the pitching moment coefficient around the force balance and then decreases it after the angles. Unlike in the two force coefficient graphs, there is no intersection point in this curve. It would mean that the sensitivity of the average pitching moment respect to flapping frequency is less than the sensitivity respect to AOA. Therefore, the force balance was tried to be installed within center of mass margin.

4.1.2 Effects of the velocity

In the study of the forces and pitching moment of the bird at a constant flapping frequency and variable speed, no unpredictable phenomenon was observed. The general trend of force coefficients variation was similar to that in the no-flapping condition (fixed wing). As shown in Fig. 8, it is related to the high-stiffness wing and the 54 deg flapping angle amplitudes and the high flexibility wing and the 72 deg flapping angle amplitudes, respectively.

4.1.3 Effects of stiffness

Figures 9 and 10 show a comparison of forces and the pitching moment coefficient due to changes in the flexibility of the main wing spar at different flapping frequencies and wind speeds at AOA of 0–80 deg. The amount of thrust minus drag force coefficients showed that this force coefficient had little difference in AOA under 40 deg in the two

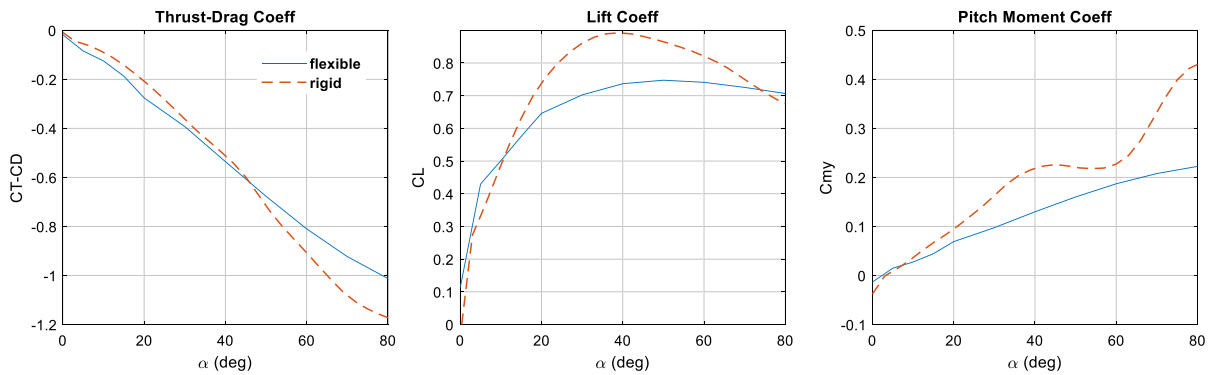


Fig. 9 Comparison of forces and pitching moment coefficient on the bird in terms of angle of attack in two flexible and rigid wing spar in the constant flapping frequency of 3 Hz and Reynolds number of 75,000

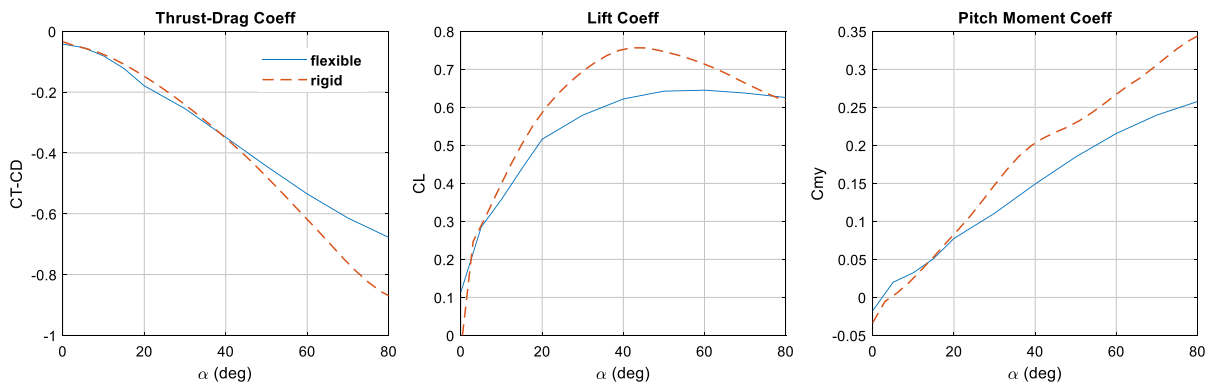


Fig. 10 Comparison of forces and pitching moment coefficient on the bird in terms of angle of attack in two flexible and rigid wing spar in the constant flapping frequency of 5 Hz and Reynolds number of 150,000

wing spars but decreased with angles above 40 deg in the rigid wing spar with a greater slope. The lift force coefficient is almost always more on the rigid wing spar than on the flexible wing spar at different AOA. The peak of this difference usually occurs at AOA of 30–50 deg.

Lift coefficient curves of the stiff and flexible wings are almost equal in the approximately 80 deg AOA when the frequency is 5 Hz. According to the pitching moment coefficient graph, it can be seen that the pitching moment coefficients are the same for two wings at lower AOA range. With increasing incident angle, the pitching moment coefficient in the rigid wing increases with steeper slope. Comparing the graphs in Figs. 9 and 10 shows that

changes in frequency and wind speed do not affect the trend of forces and the pitching moment coefficient in the two rigid and flexible wings.

4.2 Effects of flapping amplitude

The flapping amplitude of natural birds increases during landing. The effect of flapping amplitude is shown in Figs. 11 and 12. The thrust minus the drag force coefficient showed that this force coefficient was slightly higher in the 72 deg flapping range than in the 54 deg flapping range. This difference is also reduced at higher AOA. The size of the lift force coefficient is greater in the flapping range of 72 deg than in that of 54 deg. However, in contrast to the thrust force minus

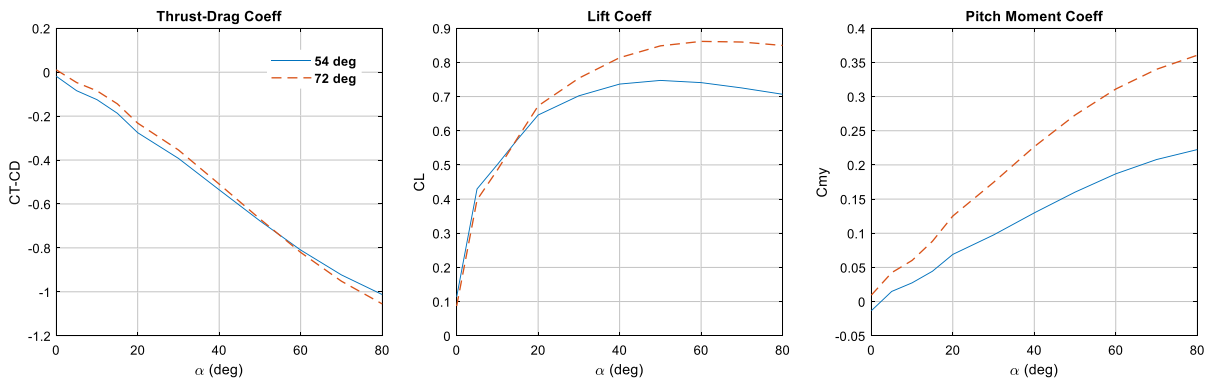


Fig. 11 Comparison of forces and pitching moment coefficient on the bird in terms of angle of attack in two different wing flapping ranges in the constant flapping frequency of 3 Hz and Reynolds number of 75,000

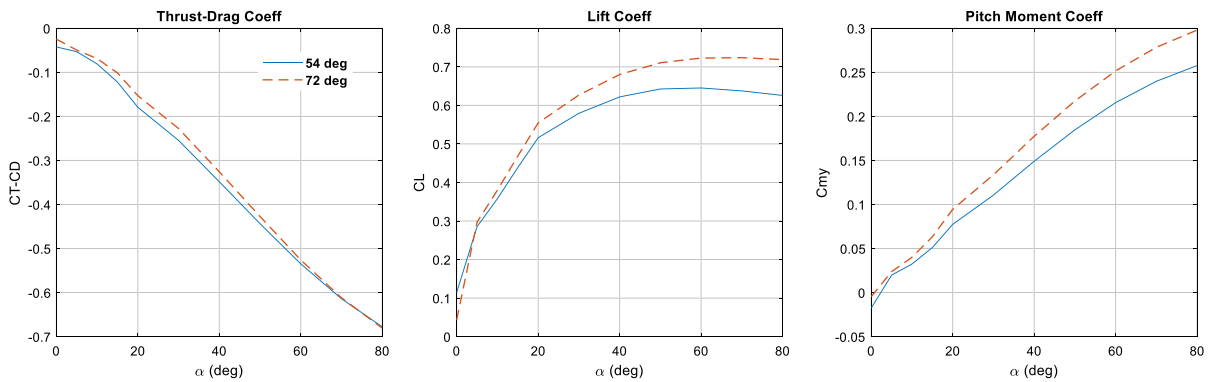


Fig. 12 Comparison of forces and pitching moment coefficient on the bird in terms of the angle of attack in two different wing flapping ranges in the constant flapping frequency of 5 Hz and Reynolds number of 150,000

the drag coefficient, the lift force coefficient differs slightly at lower AOA, and this difference increases steadily with increasing AOA. The pitching moment coefficient between the two flapping angle amplitudes has the trend of value and variation similar to that of the lift force coefficient. As can be seen from the graphs, changes in wing flapping frequency and wind speed do not affect the changing trend of forces and pitching moment.

4.3 Dynamic tests results

Dynamic tests performed in this study investigated the changes in forces and the pitching moment coefficient for the pitch rate of 36, 108, and 180 deg/s. The flapping frequency was 3, 4, 5, and 6, as can be

Table 3 Dynamic test variables and their ranges of change

Angle of attack rate $\dot{\alpha}$	Angle of attack (α)	Frequency (f)	Velocity (V)
36–108–180 (deg/s)	0–80 (deg)	3–4–5–6 (Hz)	3–5–7.5–10 (m/s)

seen in Table 3. The effect of the $\dot{\alpha}$ parameter was investigated on the results of aerodynamic data. The results of these tests are presented against both time and pitch angle. Similar to static tests, dynamic tests examined the average of forces and pitching moment data.

Figure 13 shows the results of dynamic tests with the flapping frequency of 6 Hz and Reynolds number of 150,000 at different angular velocities. As

Fig. 13 Forces and pitching moment on the bird in terms of time with the constant flapping frequency of 6 Hz and Reynolds number of 150,000 and variable angular velocities

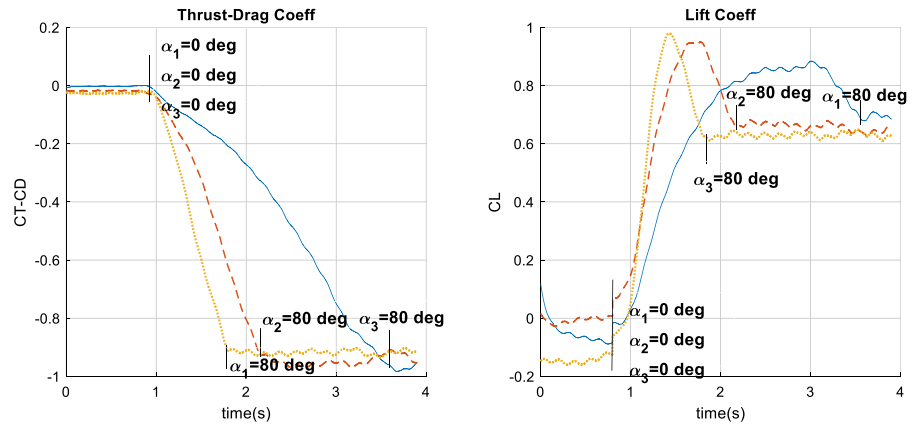
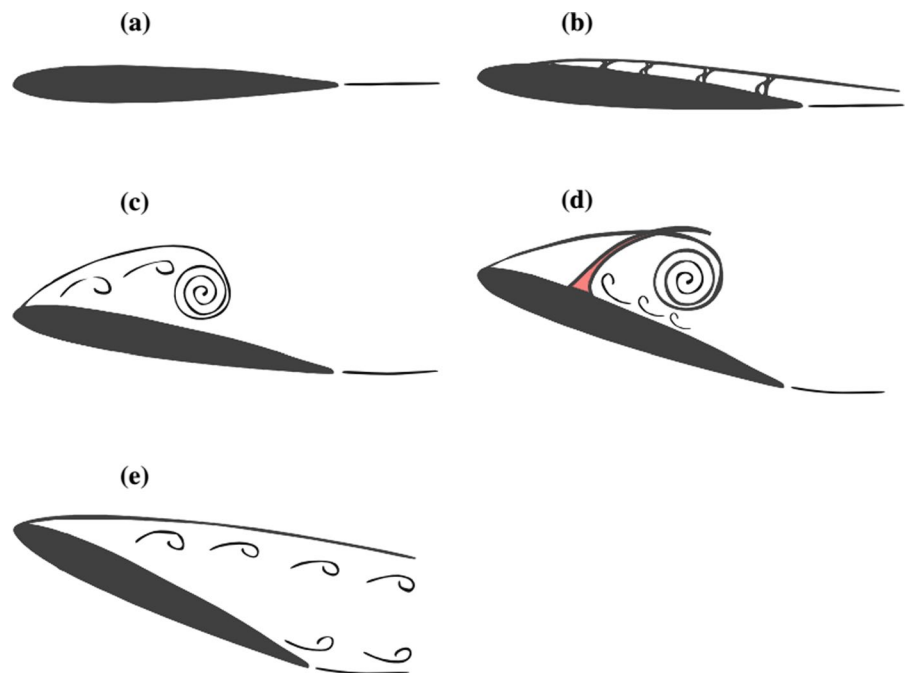


Fig. 14 Schematic representation of the different stages of the dynamic stall process. **a** Attached flow. **b** Flow reversal. **c** Shear layer roll-up. **d** Stall onset. **e** Full stall. [27]



expected, as the changing rate of AOA ($\dot{\alpha}$) increases, the interval of changes in forces and the pitching moment coefficient also decreases. As shown in Fig. 13, the test records were synchronized for all curves in such a way that the start times are the same. In each graph, the time of reaching 80 deg AOA was also specified. No significant phenomenon was observed regarding the thrust minus the drag force coefficient, but concerning the lift coefficient, a higher AOA rate, would further increase the maximum lift coefficient. This phenomenon is in fact dynamic stall which is appeared due to increase in angular velocity (Fig. 14).

In the dynamic stall phenomenon, with increasing AOA, the lift force initially increases monotonically in time, even after obtaining the maximum incidence angle. Subsequently, the force drops dramatically, eventually converging to the static stall figure. During the linear growth of the angle of incidence, the separation point moves from the trailing edge toward the leading edge. The backward displacement of the separation line is associated with the formation of a large-scale vortex on the suction side of the airfoil. The unsteady evolution of this vortex, usually termed as dynamic stall vortex, is ultimately responsible for the lift behavior. As the

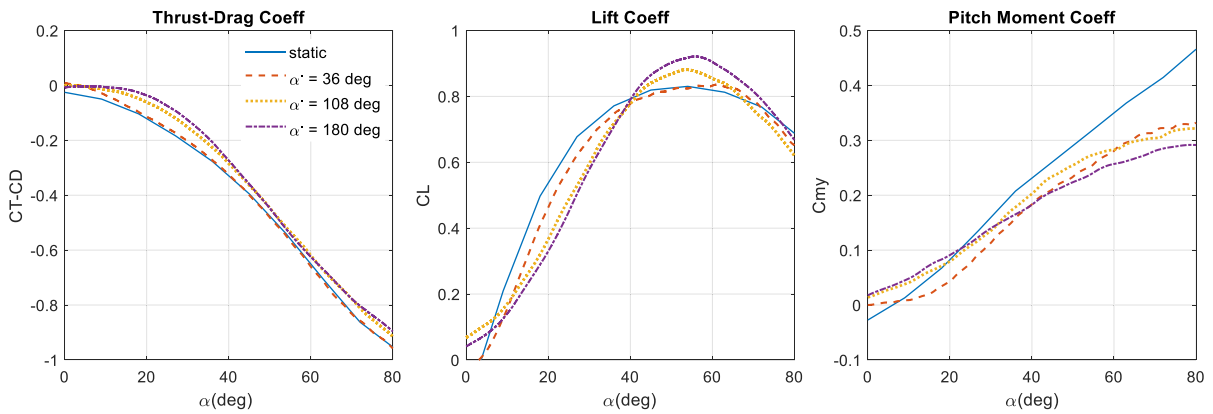


Fig. 15 Forces and pitching moment coefficient on the bird in terms of the angle of attack with the constant flapping frequency of 6 Hz and Reynolds number of 150,000 and variable angular velocities

separation line moves upstream along the suction side, vortices are generated, merged, and eventually coalesced into one large dynamic stall vortex [28].

Examining forces and the pitching moment coefficient in terms of pitch angle at different angular velocities can provide a more practical knowledge. It would better compare the behavior of the force and moment coefficient. Here, the pitch angle is the angle between the longitudinal vector of the fuselage and the longitudinal vector of the wind tunnel, and the reason for different AOA in these tests is the dynamic movement of the bird and applying a different AOA from the pitch angle. Figure 15 compares forces and the pitching moment coefficient at three different angular velocities with forces and the pitching moment coefficient in static conditions. As expected, a lower angular velocity leads to a higher force coefficient, similar to the static state. In the thrust minus drag force graph, increasing the angular velocity leads to a higher force coefficient [29].

It was revealed, increasing the angular velocity would cause a lightly increase in the average axial force. However, drag is more significant than thrust, therefore, the net values are seen to be negative. It is reminded that all curves in the Fig. 15 were measured in the frequency 6 Hz. The static label in the figure stands for the no pitching rate situation. Changes in lift force coefficient behavior due to changes in angular velocity are more significant than others. By increasing the angular velocity, a delay is observed in the graph of the force coefficient behavior relative to the static state. The maximum force coefficient

occurred near an angle of 50 deg under the above test conditions, which is equal to the inflection point of pitch angle in the thrust minus drag coefficient graph. The lift coefficient graph can be divided into three parts: a curve with an upward concavity at initial pitch angles, followed by a line at middle pitch angles and a curve with a downward concavity at final pitch angles. The upward concavity curve at initial AOA is due to the delay caused by the angular velocity not captured in the static test. The trend is the same for pitching moment.

The effect of flapping is depicted in Fig. 16. The general outcome is similar to the static test. The limit cycle graph with an angular velocity of 108 deg/s and a frequency of 4 Hz (Reynolds number 1,50,000) is plotted in Fig. 17. The static coefficients are also drawn for comparison.

5 Dimensional analysis

The rotational displacement of the wing is very close to a harmonic profile. The exact solution of the wing flapping angle for a 4-bar mechanism was presented by [30]. A simple and frequently used approximation is as follows:

$$\gamma = \frac{(\gamma_{Up} - \gamma_{Dn})}{2} \sin(2\pi ft) + \frac{(\gamma_{Up} + \gamma_{Dn})}{2} \tag{1}$$

All the three considered force and moment coefficients are a function of the parameters: flap frequency

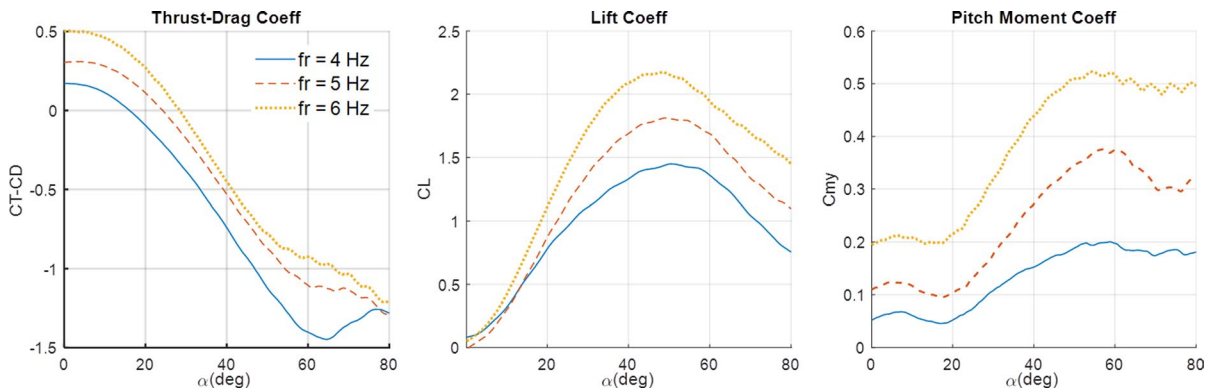


Fig. 16 Forces and pitching moment coefficient on the bird in terms of pitch angle with the constant angular velocity of 36 deg/s, Reynolds number of 75,000, and variable flapping frequencies

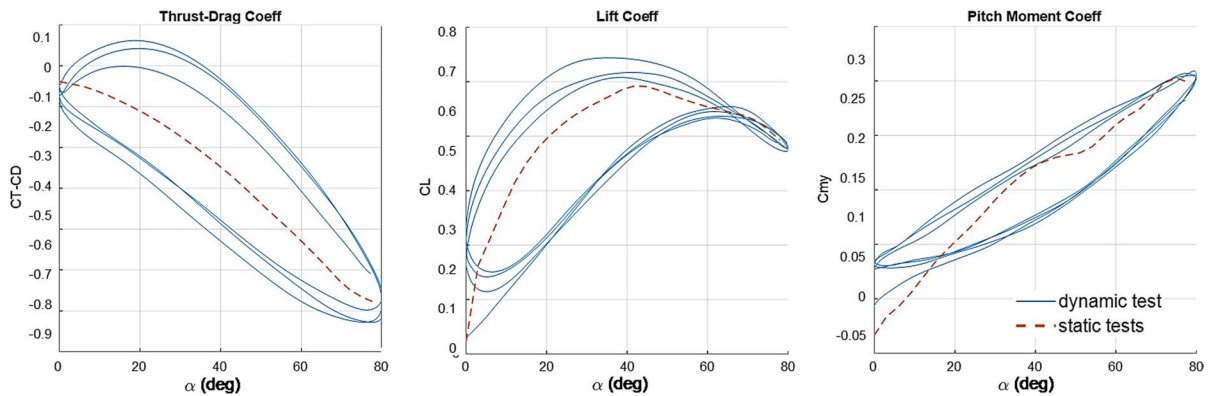


Fig. 17 Comparison of force and pitching moment coefficient graphs in terms of pitch angle in oscillating dynamic test and static tests in 4 Hz flapping frequency and Reynolds number of 150,000 and 108 deg/s angular velocity

(ω), wind speed (V), AOA (α), AOA rate ($\dot{\alpha}$), kinematic viscosity of air (ν), mean chord (C), and wing layout:

$$L = f(\omega, V, \alpha, \dot{\alpha}, \nu, c, \text{wing shape}) \tag{2}$$

$$T - D = f(\omega, V, \alpha, \dot{\alpha}, \nu, c, \text{wing shape}) \tag{3}$$

$$M = f(\omega, V, \alpha, \dot{\alpha}, \nu, c, \text{wing shape}) \tag{4}$$

The wing forward and flapping motion in the air generate variable aerodynamic forces. The reduced frequency is as follows:

$$F_R = bf / U_{ref} \tag{5}$$

It is a measure of unsteadiness. The reference velocity could be assumed as wing tip velocity [14]. For low or moderate values of F_R ($F_R < 1$), the quasi-steady assumption is valid. Producing an accurate model of forces requires the effect of all kinematic parameters. Some of the parameters have complex influences and may be ignored in this stage. Despite the significance of stiffness, it could not be addressed in this study. A series of correction coefficients were obtained using experimental data at speeds of 5, 7.5, and 10 m/s and frequencies of 3, 4, and 5 Hz, which can be implemented in semi-analytical or quasi-steady models. These coefficients are a function of

Table 4 Coefficients of Eq. 6

$P_{00} = 1.142$	$Q_{00} = 0.538$
$P_{10} = -0.252$	$Q_{10} = -0.244$
$P_{01} = 0.306$	$Q_{01} = 0.720$
$P_{20} = 0.017$	$Q_{20} = 0.021$
$P_{11} = -0.024$	$Q_{11} = -0.051$
$P_{02} = -0.003$	$Q_{02} = -0.018$

6 Landing trajectory estimation

The smooth descent phase of a typical flapping robot could be extracted based on the presented experimental data. The actual mass of the bird is 320 g. Equilibrium equations are assumed to be applied while the robot is reducing altitude. Therefore, it is supposed that the vehicle is descending gradually and smoothly. It is assumed that the bird

Fig. 18 Comparison of force data of modified band theory model with experimental data results at Reynolds number of 150,000 and a frequency of 4 Hz

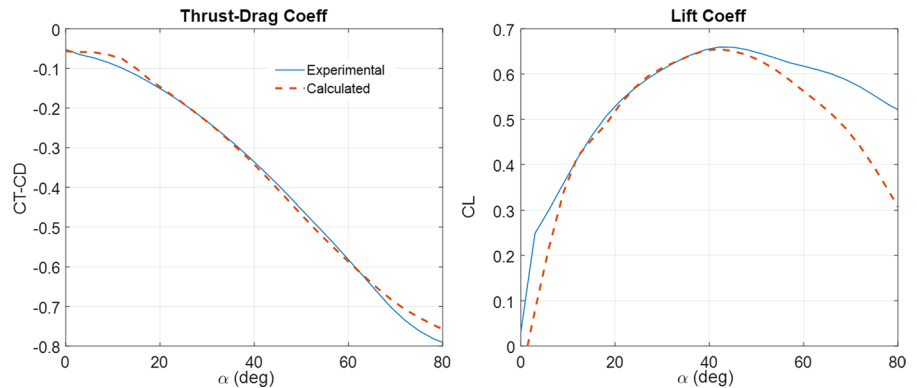
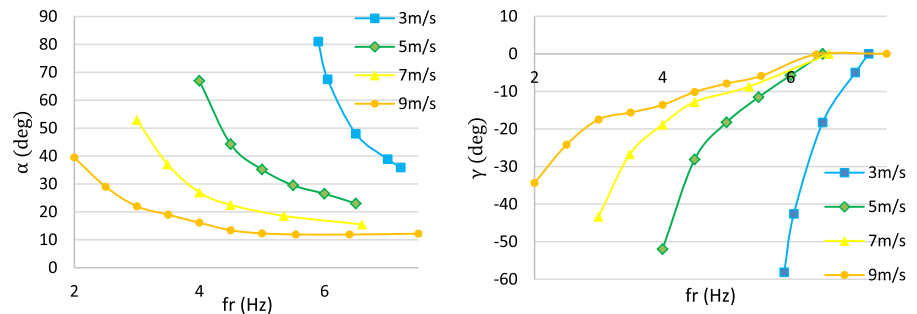


Fig. 19 Attack angle and flight path angle versus speed and frequency (the descend phase in force equilibrium condition)



the parameters related to experimental tests, shown in Eqs. 6 and Table 4. The results were obtained with data related to the frequency of 6 Hz at the speed of 3 m/s. The comparison of the estimation and experimental data is depicted in Fig. 18.

$$\begin{aligned}
 C_X(V, fr) &= P_{00} + P_{10}V + P_{01}fr + P_{20}V^2 \\
 &\quad + P_{11}V.fr + P_{02} * fr^2 \\
 C_Z(V, fr) &= Q_{00} + Q_{10}V + Q_{01}fr + Q_{20}V^2 \\
 &\quad + Q_{11}V.fr + Q_{02} * fr
 \end{aligned}
 \tag{6}$$

acceleration is small; therefore, $\dot{V} = \dot{\gamma} = 0$ and:

$$m\dot{V} = T - D - W \sin \gamma \tag{7}$$

$$-mV \gamma_2 = W \cos \gamma - L \tag{8}$$

Based on the above equations and the proposed model, a comprehensive search of the aerodynamic parameters was performed, and conditions satisfying these equations were extracted. The results of this search can be seen in Fig. 19. This diagram shows the corresponding AOA and the variation of the path angle. Also, the velocity, height, and frequency parameters were depicted in the force equilibrium

Fig. 20 Velocity and path angle in quasi-equilibrium condition

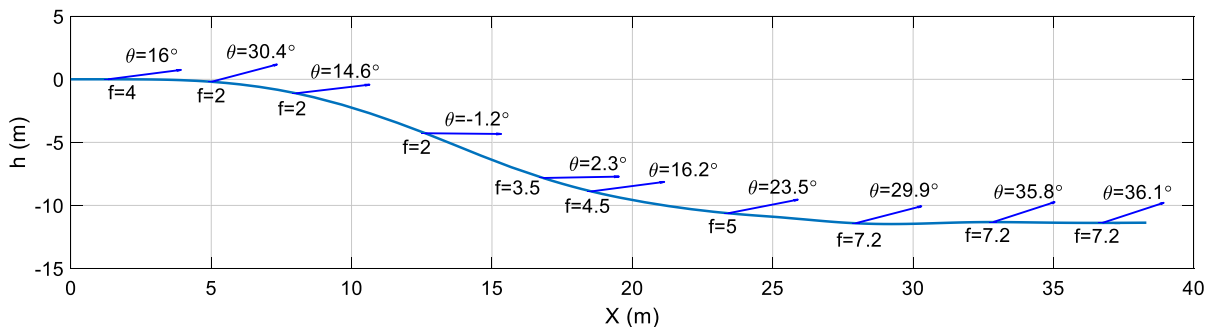
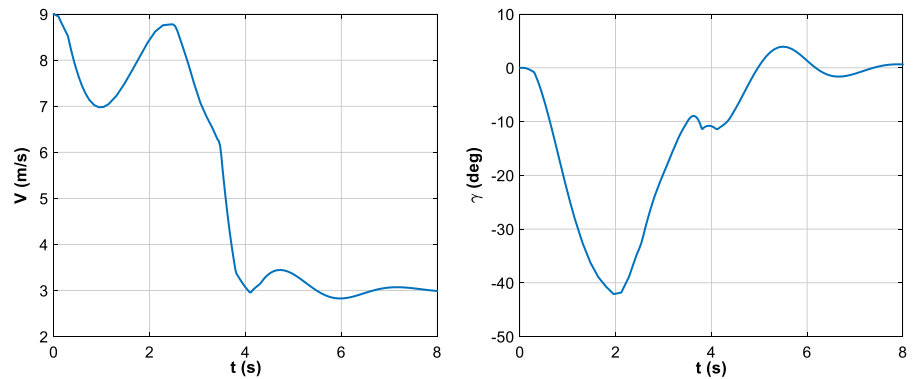


Fig. 21 Schematic depiction of descend trajectory and variation of frequency and angle of attack in terms of distance traveled

state. For example, AOA and the path angle at the frequency of 3 Hz and the speed of 9 m/s were -22 and 17.5 deg, respectively, to reduce the altitude in the force balancing mode.

With the help of the above results, different paths of quasi-equilibrium trajectories can be planned. One of the possible descend/approach paths with the help of the above data is shown in Figs. 20 and 21. The parameters shown in both figures were computed based on the quasi-equilibrium assumption. It was revealed as it was expected, by closing the bird to the terminal phase, the velocity, path angle and the level would attenuate, while the frequency and pitch angle would increase [31]. This is same as in the nature.

7 Concluding remarks

This experimental study was conducted to discover the landing and perching aerodynamics of a flapping air vehicle. In particular, the bird's high incidence angle in flapping and the angle change rate are two critical issues in landing. Therefore, static

and dynamic tests were scheduled accordingly. The parameters in the static test were selected as incidence angle, frequency, velocity, flapping range, and wing stiffness. In the dynamic test, the pitch rate also was considered. The measured quantities in both tests were normal and axial forces and pitching moment. A semi-analytical aerodynamic model, calibrated based on the experiments, was developed to study vehicle landing performance. The correction factors were adjusted to match the code results and the test data. Finally, assuming quasi-equilibrium conditions, the way-point based terminal trajectory was derived based on the aerodynamic model and the wind tunnel measurements. It was shown that an appropriate smooth schedule could be extracted using the static stand measurements for the descending maneuver of the flapping vehicle. Based on the experimental results, some critical outcomes are:

1. In lower incidence angles, a higher flapping frequency results in greater thrust, while in higher angles, this may be reversed. It is due to both

overcoming drags in high angles and changing in averaged force direction.

2. As expected, the critical angle for which the frequency-thrust coefficient relation would be switched increases by the Reynolds number. It is interesting to see the bird's deceleration in nature by flapping at high angles.
3. Considering the lift coefficient, one may conclude that in the lower and higher angles, changing the flapping frequency would lead to less and more lift coefficient, respectively. No distinct fall in the lift force coefficient was captured in the tests. Knowing that instantaneous AOA for many of the wing sections would exceed the stall margin, it may address the remarkable effects of dynamic stall and the other force generation mechanisms on the flapping environment.
4. When looking at the force coefficient variation versus Reynolds number in a fixed frequency, the normal trend may be similar to conventional air vehicles. The pitching moment coefficient almost increases by flapping frequency, meaning the control power is coupled between the wing and the tail.
5. The effect of stiffness attenuates the thrust coefficient. The thrust produced by the same flapping frequency should be higher for a more flexible wing, although it is not the case for lift force. The stiffer wing could make a bit more lift on average. The trend of pitch moment coefficient is almost similar to lift coefficient.
6. Changing the flapping range is observed to have no distinguishable effect on the overall thrust coefficient, while forming detectable changes in the lift coefficient and the moment coefficient. More lift and moment coefficients could be obtained for the 72 deg flapping range than for the 54 deg flapping range.
7. The effect of the angle rate is too complicated to be generalized. One may deduce that increasing the rotation rate produces a more significant force and the moment coefficient in the same frequency. It also causes deficiency and delay, which can be seen by hysteresis curves when a complete rotation cycle is applied.
8. The other general trend in changing the force coefficient and the moment coefficient in terms of the flapping frequency and Reynolds number seems to be the same as static behavior.

Funding No fund has been assigned to this study.

Declarations

Conflict of interest The authors declare that they have no conflict of interest.

References

1. Manzanera RJ, Smith S (2015) Flight in nature II: How animal flyers land. *Aeronaut j* 119(1213):281–299. <https://doi.org/10.1017/S0001924000010484>
2. Keennon M, Klingebiel K, Won H (2012) Development of the nano hummingbird: a tailless flapping wing micro air vehicle. In: *Aerospace sciences meetings: 50th AIAA aerospace sciences meeting including the New Horizons Forum and Aerospace Exposition*, Nashville, Tennessee, 2012, p. 85.
3. Cunis T (2016) Precision Position Control of the DelFly II Flapping-wing Micro Air Vehicle in a Wind-tunnel. In: *IEEE International Micro Air Vehicles Conference and Competition*, Beijing, China
4. de Croon GCHE, Perçin M, Remes BDW, de Wagter C, Ruijsink R (2016) *The DelFly: Design, aerodynamics, and artificial intelligence of a flapping wing robot*. Springer, Berlin.
5. Roberts LJ, Bruck HA, Gupta SK (2017) Modeling of dive Maneuvers for executing autonomous dives with a flapping wing air vehicle. *J Mechanisms Robotics* 9(6):61010. <https://doi.org/10.1115/1.4037760>
6. Shkarayev S, Silin D (2012) Measurements of aerodynamic coefficients for flapping wings at 0–90 angles of attack. *AIAA J* 50(10):2034–2042. <https://doi.org/10.2514/1.J051051>
7. Mueller D, Gerdes JW, Gupta SK (2010) Incorporation of passive wing folding in flapping wing miniature air vehicles. In: *33rd Mechanisms and robotics conference*, San Diego, California, USA, 2010, pp. 797–805.
8. Stewart EC, Patil MJ, Canfield RA, Snyder RD (2016) Aeroelastic Shape Optimization of a Flapping Wing. *J Aircr* 53(3):636–650. <https://doi.org/10.2514/1.C033278>
9. Guerrero JE et al (2016) Preliminary design of a small-sized flapping UAV: I. Aerodynamic performance and static longitudinal stability. *Meccanica* 51(6):1343–1367. <https://doi.org/10.1007/s11012-015-0298-6>
10. Negrello F, Silvestri P, Lucifredi A, Guerrero JE, Botaro A (2016) Preliminary design of a small-sized flapping UAV: II. Kinematic and structural aspects. *Meccanica* 51(6):1369–1385. <https://doi.org/10.1007/s11012-015-0309-7>
11. Nian P, Song B, Xuan J, Yang W, Dong Y (2019) A Wind Tunnel Experimental Study on the Flexible Flapping Wing With an Attached Airfoil to the Root. *IEEE Access* 7:47891–47903. <https://doi.org/10.1109/ACCESS.2019.2909916>
12. Ebrahimi A, Mazaheri K (2011) Experimental investigation on aerodynamic performance of a flapping wing vehicle in forward flight. *J Fluids Struct* 27(4):586–595. <https://doi.org/10.1016/j.jfluidstructs.2011.04.001>

13. P. Deshpande and A. Modani, “Experimental investigation of fluid–structure interaction in a bird-like flapping wing,” *Journal of Fluids and Structures*, vol. 91, p. 102712, 2019, <https://doi.org/10.1016/j.jfluidstructs.2019.102712>.
14. Mazaheri K, Ebrahimi A, Karimian S (2012) Performance Analysis of a Flapping-Wing Vehicle Based on Experimental Aerodynamic Data. *J Aerosp Eng* 25(1):45–50. [https://doi.org/10.1061/\(ASCE\)AS.1943-5525.0000102](https://doi.org/10.1061/(ASCE)AS.1943-5525.0000102)
15. X. Ke, W. Zhang, J. Shi, and W. Chen, “The modeling and numerical solution for flapping wing hovering wing-beat dynamics,” *Aerospace Science and Technology*, vol. 110, p. 106474, 2021, <https://doi.org/10.1016/j.ast.2020.106474>.
16. Gong C, Yuan Z, Fang Z, Chen G (2019) Numerical investigation of the effects of different parameters on the thrust performance of three dimensional flapping wings. *Aerosp Sci Technol* 84:431–445. <https://doi.org/10.1016/j.ast.2018.10.021>
17. Gallivan P, DeLaurier J (2007) An experimental study of flapping membrane wings. *Can Aeronaut Space J* 53:35–46. <https://doi.org/10.5589/q07-005>
18. Karimian S, Jahanbin Z (2020) Bond graph modeling of a typical flapping wing micro-air-vehicle with the elastic articulated wings. *Meccanica* 55:1263–1294. <https://doi.org/10.1007/s11012-020-01162-w>
19. Karimian S, Jahanbin Z (2019) Aerodynamic modeling of a flexible flapping-wing micro-air vehicle in the bond graph environment with the aim of assessing the lateral control power. *Proceedings of the Institution of Mechanical Engineers, Part G: Journal of Aerospace Engineering* 233(13):4998–5015. <https://doi.org/10.1177/0954410019835980>
20. Wickenheiser AM, Garcia E (2008) Optimization of perching Maneuvers through vehicle morphing. *J Guid Control Dyn* 31(4):815–823. <https://doi.org/10.2514/1.33819>
21. Wickenheiser AM, Garcia E (2006) Longitudinal Dynamics of a Perching Aircraft. *J Aircr* 43(5):1386–1392. <https://doi.org/10.2514/1.20197>
22. Hoburg RW (2009) System Identification of Post Stall Aerodynamics for UAV Perching. In: *AIAA guidance navigation and control conference and exhibit*, Seattle, Washington
23. Cory RR (2008) Experiments in fixed-wing UAV perching. In: *AIAA Guidance Navigation and Control Conference and Exhibit*, Honolulu, Hawaii, pp 1–12.
24. Moore JL (2011) Powerline Perching with a Fixed-Wing UAV. MSc Thesis, Massachusetts Institute of Technology
25. Puopolo M, Reynolds R, Jacob J (2013) Comparison of three aerodynamic models used in simulation of a high angle of attack UAV Perching Maneuver. In: *51st AIAA Aerospace Sciences Meeting including the New Horizons Forum and Aerospace Exposition*.
26. Puopolo M, Jacob JD (2015) Model for longitudinal Perch Maneuvers of a fixed-wing unmanned aerial vehicle. *J Aircr* 52(6):2021–2031. <https://doi.org/10.2514/1.C033136>
27. Reich GW, Eastep FE, Altman A, Albertani R (2011) Transient poststall aerodynamic modeling for extreme Maneuvers in micro air vehicles. *J Aircr* 48(2):403–411. <https://doi.org/10.2514/1.C000278>
28. Rosti ME, Omidyeganeh M, Pinelli A (2016) Direct numerical simulation of the flow around an aerofoil in ramp-up motion. *Phys Fluids* 28(2):25106. <https://doi.org/10.1063/1.4941529>
29. Mulleners K, Raffel M (2013) Dynamic stall development. *Exp Fluids* 54(2):403. <https://doi.org/10.1007/s00348-013-1469-7>
30. Pourtakdoust SH, Karimain Aliabadi S (2012) Evaluation of flapping wing propulsion based on a new experimentally validated aeroelastic model. *Sci Iran* 19(3):472–482. <https://doi.org/10.1016/j.scient.2012.03.004>.
31. Karimian S, Ebrahimi A (2014) Parametric study for kinematic optimization of flapping wing air vehicle using a new aeroelastic model. *Modares Mech Eng J* 14(9):73–80 (in Persian)

Publisher’s Note Springer Nature remains neutral with regard to jurisdictional claims in published maps and institutional affiliations.

Springer Nature or its licensor (e.g. a society or other partner) holds exclusive rights to this article under a publishing agreement with the author(s) or other rightsholder(s); author self-archiving of the accepted manuscript version of this article is solely governed by the terms of such publishing agreement and applicable law.